

SYNKINEMATIC INTRUSION OF PERALUMINOUS AND ASSOCIATED METALUMINOUS GRANITIC MAGMAS, WHIPPLE MOUNTAINS, CALIFORNIA

J. LAWFORDE ANDERSON AND MARK C. ROWLEY

*Department of Geological Sciences, University of Southern California,
Los Angeles, California 90007, U.S.A.*

ABSTRACT

The autochthon of the Whipple Mountains detachment terrain (California) contains two generations of peraluminous intrusive bodies, each one coeval with a distinct metamorphic event. Garnet-biotite granodiorite and two-mica adamellite plutons were generated during an early ductile metamorphism. Subsequent Late Cretaceous mylonitization was synchronous with the intrusion and formation of a sheeted sill complex. Peraluminous sills, which contain two-mica tonalite and garnet-two-mica granodiorite, form a major central portion of the compositionally zoned sill complex. The structurally uppermost and lowermost sills, composed of biotite granodiorite and hornblende-biotite quartz diorite, respectively, are metaluminous. The primary white mica in the peraluminous rocks contains 19.5–32.5% of a titaniferous ferriceladonite end-member, $K(Mg_{0.8}Ti_{0.2})Fe^{3+}(Si_{3.6}Al_{0.4})O_{10}(OH)_2$. Chemographic analysis shows that these celadonitic muscovites are consistent with shallow levels of intrusion; a depth of 9.6–11.5 km is calculated. Shallow depth is also suggested by the Mn-rich composition of garnet, which contains 42.6–47.4 mole % almandine, the remainder being comprised primarily of subequal proportions of spessartine and grossular. Biotite compositions indicate crystallization under fairly oxidizing conditions (Ni–NiO to MnO–Mn₃O₄ buffer curves), an inference consistent with the abundance of magnetite and the near-absence of ilmenite. These peraluminous intrusive rocks are thus set apart from S-type granitoid rocks. The composition of the magmas that generated the older and younger peraluminous suites is only weakly alumina-saturated when compared with S-type granitoid rocks of other orogenic belts; this is due to a high content of Na and Ca, not to low Al. The marked similarity of melts coeval with the metamorphic events is indicative of crustal anatexis involving exceedingly similar source materials. Although fractional crystallization was dominated by plagioclase, the removal of hornblende or allanite (or both) performed a major role in increasing the peraluminous nature of one intrusive body.

Keywords: two-mica granite, Cordilleran metamorphism, Whipple Mountains, California, muscovite, biotite, garnet, mylonitization.

SOMMAIRE

Le complexe autochtone des montagnes Whipple (Californie) contient deux générations de roches intrusives hyperalumineuses, chacune associée à un événement métamorphique distinct. Les massifs de granodiorite à grenat et biotite et d'adamellite à biotite et muscovite ont été mis en place pendant un premier épisode de métamorphisme, à caractère ductile. Une mylonitisation au Crétacé supérieur a accompagné l'intrusion d'un complexe feuilleté de sills. La plus grande partie centrale du complexe zoné contient des sills de composition hyperalumineuse, qui comprennent: tonalite à biotite et muscovite et granodiorite à grenat, biotite et muscovite. Les sills supérieur et inférieur, composés respectivement de granodiorite à biotite et diorite quartzifère à hornblende et biotite, sont de composition métallumineuse. Le mica blanc primaire dans ces roches hyperalumineuses contient de 19.5 à 32.5% d'un pôle celadonitique ferrifère et titanifère, $K(Mg_{0.8}Ti_{0.2})Fe^{3+}(Si_{3.6}Al_{0.4})O_{10}(OH)_2$. D'après une analyse chimographique, ces muscovites celadonitiques sont compatibles avec une mise-en-place à faible profondeur; le calcul donne 9.6 – 11.5 km. Cette profondeur est aussi indiquée par la composition manganesifère du grenat, qui contient de 42.6 à 47.4% (molaire) d'almandin et, en proportions à peu près égales, les pôles spessartine et grossulaire. La composition des biotites indique une cristallisation en milieu relativement oxydant, près des tampons Ni–NiO et MnO–Mn₃O₄, ce qui expliquerait l'abondance de magnétite et l'absence quasi-totale d'ilménite. Ces roches se distinguent donc des roches granitoïdes de type S. La composition du magma dans les deux associations n'est que légèrement saturée en Al₂O₃ en comparaison des roches granitoïdes de type S provenant d'autres ceintures orogéniques; ceci serait l'expression d'une haute teneur en Na et Ca plutôt que d'une déficience en Al. La grande ressemblance des magmas formés lors des deux épisodes métamorphiques résulterait d'une anatexis de croûte à caractère uniforme. Quoique le plagioclase ait été le produit dominant de la cristallisation fractionnée de ces magmas, la séparation de la hornblende ou de l'allanite (ou des deux) a joué un rôle important dans le développement du caractère hyperalumineux d'un des massifs.

(Traduit par la Rédaction)

Mots-clés: granite à deux micas, métamorphisme de la Cordillère, muscovite, biotite, grenat, mylonitisation, montagnes Whipple, Californie.

INTRODUCTION

The polymetamorphic complex comprising the autochthon of the Whipple Mountains and adjacent ranges in southeastern California is representative of similar complexes existing southeastward across Arizona and into Sonora, Mexico (Fig. 1). They are part of a belt of Cordilleran Mesozoic to Tertiary metamorphic complexes that trend south from British Columbia (Davis & Coney 1979). The complexes in the southern group, including that of the Whipple Mountains, share several similarities: (1) a low-angle mylonitic foliation containing a ubiquitous northeast-trending mineral lineation, (2) spatial association of metamorphism with the intrusion of synkinematic and late-kinematic granites that are commonly peraluminous in composition (Keith *et al.* 1980, Haxel *et al.* 1980), (3) upward termination of the complexes at a Miocene low-angle detachment fault and associated zone of brecciation and chloritic alteration, (4) late doming of the ranges, exposing the detachment fault around the periphery and the metamorphic complex in the core of the range.

The subject of this paper is the evolution of peraluminous and associated metaluminous granitic magmas coeval with two metamorphic events in the autochthon of the Whipple Mountains. The younger event, mylonitic in nature, is Late Cretaceous in age (Davis *et al.* 1980, Martin *et al.* 1980, R.L. Armstrong, in prep.). In contrast, the earlier event was more ductile and, although perhaps Precambrian, it may be Jurassic to mid-Cretaceous, based on (1) ages of similar ductile metamorphism in this region (see summary in DeWitt 1980) and (2) striking compositional similarity between this and the subsequent intrusive episode, which was synkinematic with the later mylonitization.

GEOLOGICAL SETTING

A detailed description of the Whipple Mountains and adjacent ranges has been reported by Davis *et al.* (1980) and Anderson *et al.* (1979a). Dividing this and adjacent ranges into upper and lower plates is a through-going low-angle detachment fault that juxtaposes strikingly different lithologic assemblages. Kinematic indicators suggest the northeasterly transport of an upper plate (Davis *et al.* 1980) composed largely of Precambrian crystalline units overlain unconformably by Tertiary volcanic and

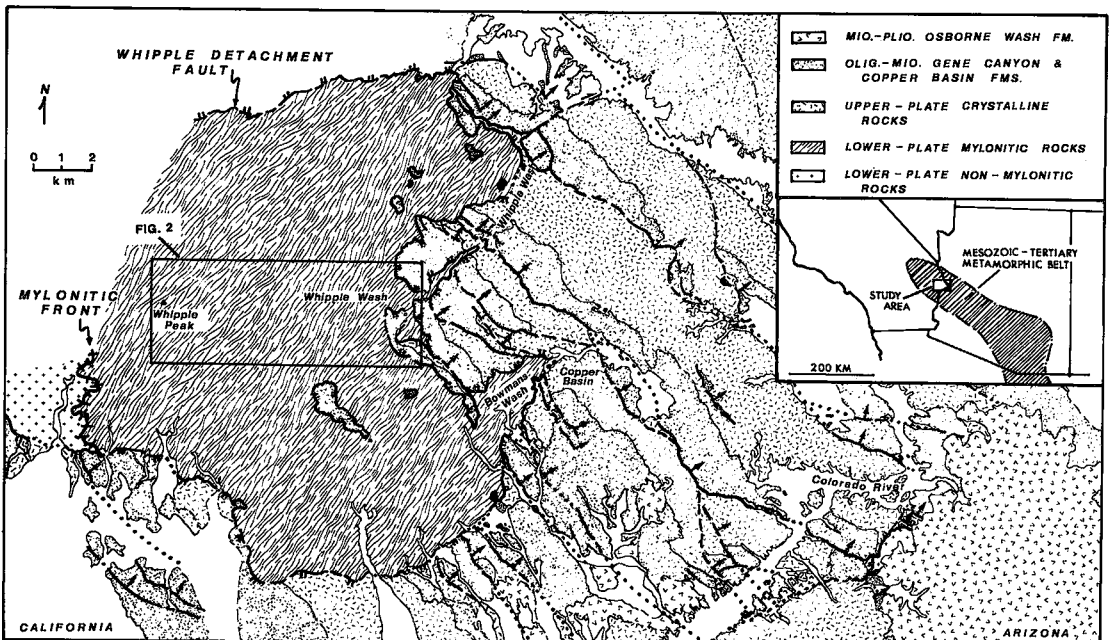


Fig. 1. Generalized geological map of the Whipple Mountains, southeastern California (from Davis *et al.* 1980).

sedimentary rocks. The crystalline lithologies include red, potassic, iron-enriched Precambrian granitic units that are intrusive into an older Precambrian metamorphic complex (Podruski 1979, Anderson *et al.* 1979b, Krass 1980). Although Jurassic resetting of K-Ar dates (biotite, hornblende) in the upper plate is widespread (D. Krummenacher, pers. comm. 1980), the effects of the Late Cretaceous metamorphism common to the lower plate are conspicuously absent.

The lower plate is composed principally of mylonitic gneisses that have a characteristic low-angle mylonitic foliation and northeast-trending lineation, the result of the Late Cretaceous metamorphic event. The protoliths of the mylonitic gneisses include (1) granitic and commonly peraluminous sills intruded synkinematically with mylonitization, (2) older peraluminous granitoid rocks intruded during an earlier metamorphism and (3) the country-rock gneisses.

These units do not occur in an upper-plate position in this or any nearby range.

DESCRIPTION OF LOWER-PLATE METAMORPHIC AND INTRUSIVE UNITS

Country-rock gneisses

The host rocks for both peraluminous intrusive suites are amphibolite-grade, banded quartzofeldspathic gneiss, augen gneiss, amphibolite, garnet-kyanite-biotite-muscovite schist and, at the deepest levels, a quartz-two-feldspar biotite schist. Local migmatization within these units is common. Ongoing field studies suggest that the above lithologies have experienced an even earlier, Precambrian (?) metamorphism. Isotopic studies are in progress to evaluate this preliminary conclusion, but as this event did not involve the intrusion of peraluminous melts, it will not be treated further in this paper.

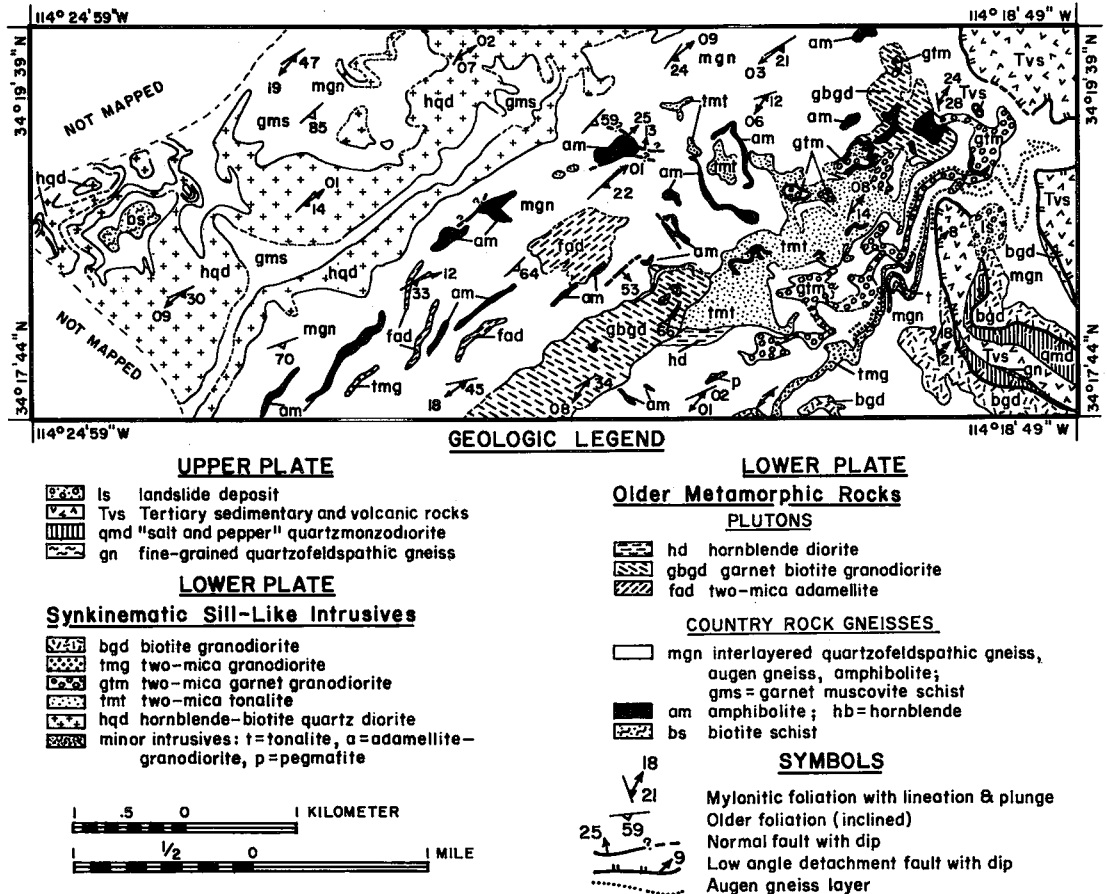


FIG. 2. Simplified geological map of the central Whipple Mountains.

Older peraluminous plutons

Intrusive into the gneisses and, in turn, cut by the sills described below are bodies of garnet-biotite granodiorite and two-mica adamellite (Fig. 2). Where the premylonitization fabric has been preserved, these plutons share the same steep northeast-striking, southwest-dipping (60–75°) foliation of the country-rock gneisses.

The garnet-biotite granodiorite is strongly to moderately foliated and is medium- to coarse-grained and inequigranular to porphyritic, with development of scattered plagioclase phenocrysts. Grey in color, the rock has a range in color index of 7.0 to 15.5, with biotite as the dominant mafic phase. Garnet occurs as conspicuous crystals (3–6 mm) in intermediate to more felsic members. Interestingly, hornblende occurs in minor amounts with biotite in the more mafic members, whereas muscovite occurs in the more felsic members. As shown below, the pluton has a dramatic and systematic range in chemistry, changing from metaluminous to peraluminous compositions with increasing

silica. The modal composition (Fig. 3) ranges from tonalite to adamellite, with the majority falling in the granodiorite field. We interpret this foliated pluton as synkinematic with the earlier ductile metamorphism, as it intruded into the plane of this earlier fabric.

More discordant and plug-like in shape is the foliated two-mica adamellite (*fad*, Fig. 2). A very similar intrusive body has been mapped by G.A. Davis above the mylonitic front (see Fig. 6 of Anderson *et al.* 1979a) in the southwest region of the range. The rock is medium- to fine-grained, light grey in color, with subequal proportions of biotite and muscovite, together comprising 5.7–10.4% of the rock. The rock generally is uniform in composition but ranges from adamellite (predominant) to granodiorite. Although the pluton shares the steep foliation of the gneisses (where not mylonitized), it is not highly recrystallized, and its more discordant nature relative to the other plutons suggests that it may be syn- to late-kinematic relative to the early metamorphism.

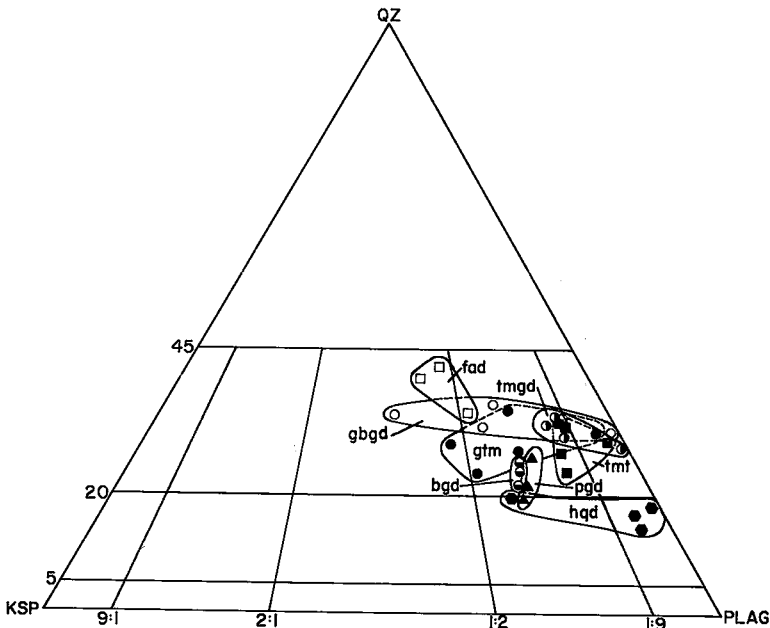


FIG. 3. Modal composition of synkinematic sills and older plutons. Symbols for the synkinematic sills: *pgd* ▲ porphyritic biotite granodiorite, *bgd* ● biotite granodiorite, *tmgd* ● two-mica granodiorite, *gtm* ● garnet-two-mica granodiorite, *tmt* ■ two-mica tonalite and *hgd* ● hornblende-biotite quartz diorite. Symbols for the older plutons: *gbgd* ○ garnet-biotite granodiorite and *fad* □ two-mica adamellite. The IUGS classification (Streckeisen 1976) is used throughout, with a single modification: a subdivision of the granite field into two areas, granite and adamellite.

Mylonitization and development of a sheeted sill complex

Throughout much of the lower plate, the fabric of these older metamorphic rocks is thoroughly overprinted by the effects of the subsequent Late Cretaceous metamorphism, a severe semiductile, semibrittle mylonitic event. The effects of mylonitization are generally structurally truncated at the overlying detachment fault except in the southwestern region of the range where mylonitic rocks pass upward into nonmylonitic rocks through a "mylonitic front" (Davis *et al.* 1980), a discrete 3–30 m zone of structural transition. The minimum structural thickness of the mylonitized section is 3.9 km.

This metamorphism is termed mylonitic owing to the brittle behavior exhibited by many of the minerals, which occur both as broken porphyroclasts and as finely comminuted material in a variably recrystallized matrix. A lineation is defined by flattened and strongly elongated quartz and by trains of broken biotite, amphibole and feldspar porphyroclasts. Dispersed porphyroclasts of plagioclase and lesser amounts of epidote, allanite, garnet, biotite, muscovite, sphene, apatite and magnetite disrupt the fine grained, strongly foliated, comminuted and partly recrystallized matrix. Within the matrix, segregated monomineralic lenses of more ductile quartz and alkali feldspar separate bands of very fine-grained granoblastic plagioclase + mica + epidote. This metamorphism was generally of middle- to upper-greenschist grade but reached lower amphibolite in the deepest structural levels.

An intrinsic feature of the mylonitization was that cataclasis was accompanied by retrogression. With the exception of epidote, new minerals were not formed, and partial re-equilibration of minerals in the older metamorphic rocks and plutons and the sills described below was highly restricted. Aspects of this retrogression are summarized in a separate section below and are being treated in a separate paper on mineral re-equilibration with mylonitization (Anderson, in prep.). The upper 2.6 km of the mylonitized section was pervaded by forcefully injected synkinematic sills or sheets of granitic composition ranging in thickness from less than a metre to several hundred metres. On a local scale, contacts are sharp, but *lit-par-lit* injection zones of sill and country-rock gneiss or older pluton are very common. Narrow chill zones along the margins of the sills occur but are not well developed.

For the major sills, there is a compositional change with structural position. In general, there is a decrease in SiO₂ and an increase in the color index with increasing depth. Metaluminous intrusive bodies are confined to the uppermost and lowermost structural levels, with the highest two sills being biotite granodiorite and the lowest sill a hornblende–biotite quartz diorite. Peraluminous intrusive bodies occupy the central section of this sheeted sill complex and include, from top to bottom, a two-mica granodiorite, a garnet–two-mica granodiorite and a two-mica tonalite.

We consider these sills, although strongly mylonitized, to be synkinematic with mylonitization for the following reasons. (1) They have intruded as nearly horizontal sheets parallel to the mylonitic foliation and compositional layering of the older gneisses. (2) They are restricted to structural levels below the mylonitic front. (3) The sills and adjacent gneisses are commonly more mylonitized than gneisses further from the sills. It is not uncommon to find relict, steep foliation of the earlier metamorphism preserved between the sills. Toward a sill–gneiss contact, this steep foliation becomes rotated, with coincident development of the low-angle mylonitic foliation and lineation. (4) The interior of some peraluminous sills is pegmatitic and only weakly mylonitized. (5) Some of the late aplite and tonalite sheets are slightly discordant to the mylonitic fabric of the major sills, and yet are mylonitized not in the plane of the larger sills but in their own plane of intrusion. The mylonitic fabric of the larger sills is sharply rotated into parallelism at the contact with the fabric of the smaller sheets, the lineation being the same for both mylonitic foliations.

The above metamorphic rocks are intruded discordantly by late-kinematic plutons of biotite quartz diorite to adamellite that locally possess a weak equivalent of the same mylonitic foliation and lineation. Studied by Krass (1980) and Thurn (1980), these plugs are lithologically and compositionally similar to scattered, weakly peraluminous biotite adamellites that are intrusive into the Precambrian terrain of the upper plate and that possess K/Ar dates (on biotite) ranging from 78 to 82 Ma (Davis *et al.* 1980).

Synkinematic sills

Each of the major sills is lithologically distinct. The two structurally highest sills are metaluminous biotite granodiorites and are modally quite similar (Fig. 3). The higher of the two is equigranular, medium grained and generally light in color (color index 5.1–6.7). It reaches

a maximum thickness of 600 m, but owing to its high structural position, it is generally truncated by the detachment fault, as shown in Figure 2. At a similar but slightly lower structural level in the southwestern region of the range is a porphyritic granodiorite sill that occurs 250 m below the mylonitic front (see Figs. 10 and 11 of Davis *et al.* 1980). The sill reaches a maximum thickness of 500 m and is also medium grained, with scattered alkali feldspar phenocrysts (0.3–1.2 cm, 12–18%). Biotite is the only mafic phase in both intrusive bodies, and sphene is a distinctive accessory mineral along with allanite, magnetite, apatite and zircon.

Below the upper metaluminous sills is the major zone of peraluminous sills. The section is about 600 m thick, and three major sills make up at least 64% of the section. The two upper sills are leucocratic, medium grained granodiorites (color index 4.0–7.6). Both have two micas, biotite (2.0–6.2%) and celadonic muscovite (1.0–3.1%); one distinction is the conspicuous presence of garnet only in the lower of the two. Accessory minerals include allanite (commonly overgrown with secondary epidote formed during mylonitization), magnetite, apatite and zircon. Both sills are 50–75 m thick.

The lowest peraluminous sill of two-mica tonalite is the thickest of the three (270 m). The sill was intruded at the same structural level as the older garnet–biotite granodiorite, and lenses of this older pluton and amphibolite are common inclusions in the sill. Fine- to medium-grained, the rock is dark grey in color and has a modal composition that straddles the granodiorite–tonalite boundary. The color index is high (6.9–13.2), reflecting the high content of biotite (5.6–12.5%) relative to muscovite (0.1–0.8%). Allanite, magnetite, apatite, zircon and, rarely, garnet are accessory minerals.

The deepest sills occur in proximity to the central high ridge of the Whipple Mountains (Fig. 2) and are all of the same hornblende–biotite quartz diorite body. Together, the sills are 480 m thick and structurally occur 920 m below the two-mica tonalite. The rock is medium grained and is composed primarily of plagioclase (43.5–52.9%) and prismatic hornblende (20.3–28.2%). Interstitial quartz (12.0–14.5%) and alkali feldspar (0.5–15.4%) occur in lesser amounts. Biotite is commonly also present (2.6–11.1%), with higher proportions forming as a secondary mineral after hornblende. Epidote (1.7–5.4%) is likewise a prominent secondary mineral.

Numerous smaller sills and low-angle dykes

(thickness less than a metre) of biotite tonalite and trondhjemitic aplite intrude the above sills and older plutons and gneisses. Both are very fine-grained and commonly have small porphyroclasts (1–2 mm) of relict plagioclase phenocrysts with delicate oscillatory zoning well preserved. The tonalites are grey and contain biotite \pm minor muscovite. The aplites are generally devoid of dark minerals (except for magnetite) and contain small amounts of both primary and secondary muscovite.

ANALYTICAL PROCEDURE

Electron-microprobe analyses of plagioclase, alkali feldspar, biotite, muscovite, hornblende, garnet, allanite, epidote, sphene, and magnetite were carried out on an automated 3-channel M.A.C. microprobe at the California Institute of Technology. Simple oxides and well-characterized silicate minerals were used as standards. The scheme of Bence & Albee (1968) was used for data reduction, with the alpha factors of Albee & Ray (1970). Operating conditions included a 15 kV accelerating potential, with a 0.05 mA beam current set on brass and 2–20 μ m beam diameter.

Analyses of nine major elements, Rb, Sr and Ba were done by atomic absorption on 45 rock samples from all intrusive units. Dissolution was done in a teflon-lined bomb by a method modified after that of Bernas (1968). Synthetic multielement standards were used; the U.S.G.S. and G.S.C. samples G-2, SY-2 and W-1 were analyzed as internal standards with each batch of samples. Replicate analyses of these known samples by our laboratory show an uncertainty of less than 0.6% (relative) for concentrations greater than 1.0%, an uncertainty of 0.6–2.3% (relative) for concentrations in the range of 1.0% and 1000 ppm, and 1–5% (relative) for trace elements less than 1000 ppm. Loss on ignition (L.O.I.) is volatile loss at 1000°C, reported in wt. %.

Modal analyses were done by point counting of feldspar-stained thin sections (1000 counts minimum).

MINERALOGY AND CONDITIONS OF CRYSTALLIZATION

Effects of mylonitization

Since every intrusive body is highly mylonitized, the effects of this metamorphism on the original igneous compositions constitute an additional complication. Detailed electron-micro-

probe work was done on 21 samples from all intrusive bodies in an effort to separate primary from metamorphic compositions. Numerous analyses were done on the dual textural habits (porphyroclast *versus* mylonitic matrix) that most minerals have in any sample.

Remarkably, the composition of most of the minerals was not affected by the mylonitization, despite strong effects of its penetrative deformation. The fact that plagioclase porphyroclasts have well-preserved, rather delicate oscillatory zoning gave us our initial clue to this fact. For many minerals, we have been able to document bimodal compositions commonly following the lines of the textural division (porphyroclast *versus* matrix). Only magnetite (the only Fe-Ti oxide phase in the sills) and alkali feldspar have generally been thoroughly re-equilibrated to near end-member compositions (*i.e.*, Mt_{88-99} and Or_{88-94} , respectively). Bimodal compositions

have been documented for plagioclase, biotite and muscovite. Garnet has not been compositionally affected by mylonitization. Hence, primary compositions, once detected, can be utilized to place constraints on the conditions of igneous petrogenesis; likewise, retrograded compositions provide a basis for evaluating conditions during mylonitization.

The retrogression of plagioclase led either to sodic oligoclase or to albite. The generation of epidote, which occurs either as coarse overgrowths on primary allanite or as small grains in the mylonitic matrix, testifies to this retrogression. Primary plagioclase compositions vary systematically with rock type. In the older plutons, primary plagioclase has the composition $An_{22.9-29.5}$ in the garnet-biotite granodiorite and $An_{21.2-25.0}$ in the two-mica adamellite. In the sills, primary plagioclase has the composition $An_{25.2-32.0}$ in the two-mica tonalite and decreases to

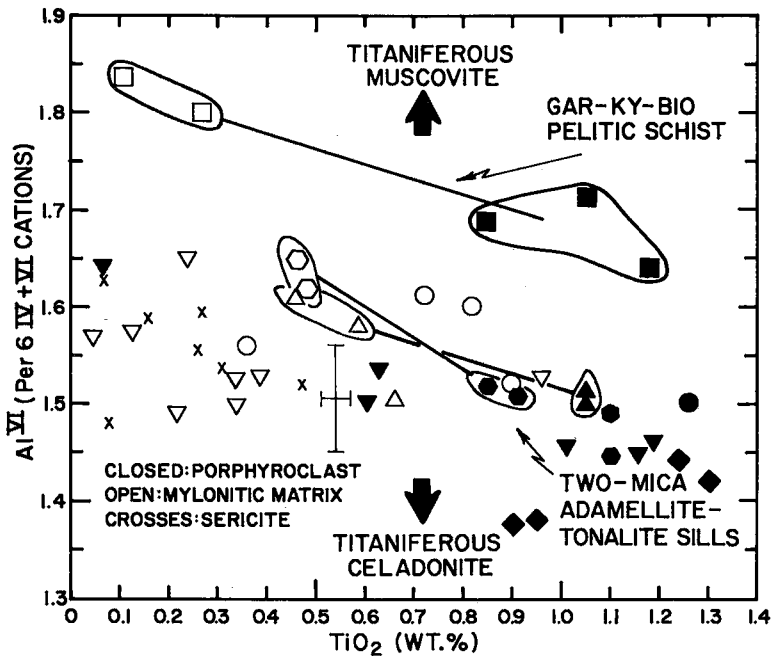


FIG. 4. Composition of muscovite from two-mica-bearing intrusive rocks and pelitic schist of country-rock gneisses in terms of octahedral Al and wt. % TiO_2 . Error bar represents two standard deviations derived from precision on Al, Si and Ti determinations. Note the high TiO_2 of most specimens of porphyroclastic muscovite relative to matrix muscovite, the similarity of matrix muscovite to sericite (Anderson, unpubl. data), the celadonitic nature (low Al^{VI}) of igneous muscovite and the decrease in celadonite content with mylonitization (negative correlation of Al^{VI} and TiO_2). Symbols for the synkinematic sills: Δ, \blacktriangle two-mica granodiorite, $\nabla, \blacktriangledown$ garnet-two-mica granodiorite, \circ, \bullet two-mica tonalite, \square, \blacksquare trondhjemitic aplite. Symbols for the older plutons: \blacklozenge garnet-biotite granodiorite, \bullet two-mica adamellite.

An_{17.6-26.2} in the more felsic granodiorite sills and An_{9.4-12.6} in the trondhjemitic aplites.

For the two micas, the most dramatic change with retrogression took place in the TiO₂ content. Other elemental changes occurred largely to compensate for the change in Ti, which in some specimens exceeds an order of magnitude. Empirical studies in natural systems (for both biotite and muscovite) and experimental studies in pure systems (for biotite) have documented well the sensitive temperature-dependence of Ti solubility in both micas (Guidotti *et al.* 1976, Robert 1976, Anderson 1980).

Muscovite

The most distinctive compositional feature of muscovite in all of the two-mica-bearing intrusive bodies (older plutons and synkinematic sills) is the content of a titaniferous ferriceladonite end-member. Celadonitic muscovite (or phengite) is commonly regarded as a product of low-temperature or high-pressure crystallization (Ernst 1963, Velde 1965, 1967, 1972). To discern magmatic from metamorphic or secondary white mica, we have attempted to fully characterize compositionally all textural forms of muscovite in the two-mica intrusive rocks. As noted above, our microprobe studies showed that Ti is a particularly sensitive parameter in distinguishing primary from secondary muscovite. Figure 4 exhibits the effects of mylonitization on muscovite, showing that TiO₂ in porphyroclasts of muscovite (large kinked flakes interrupting the flow of the fine-grained foliated matrix) is markedly higher relative to muscovite in the matrix. Matrix muscovite closely approaches the composition of sericite taken from other studies of granitic rocks (Anderson, unpubl. data) and is certainly a retrograded composition in view of the studies by Guidotti *et al.* (1976). Evidently the muscovite porphyroclasts (like the other porphyroclast phases in these intrusive rocks) have retained a magmatic composition. With retrogression during mylonitization, muscovite is depleted in Ti, Mg, Fe and Si and enriched in Al^{VI} and Al^{IV}, suggesting a coupling of the solution mechanisms $Ti + R^{2+} = 2Al^{VI}$, $Si + R^{2+} = Al^{IV} + Al^{VI}$ and $Fe^{3+} = Al^{VI}$. Hence, during retrogression, muscovite becomes less celadonitic, which is shown by the negative correlation of data depicted in Figure 4. Although similar decreases in celadonite content have also been reported elsewhere (Anderson *et al.* 1980), other workers (Miller *et al.* 1981) have noted no change or even an increase in celadonite content. As implied by Guidotti & Sassi (1976), this variable behavior in celadonite

solution with subsolidus retrogression may be the result of differing depths of emplacement: at moderate or greater depths, the celadonite content may increase with decreasing temperature, and yet with shallow depths there may be no change or even a decrease in celadonite solution. In common with all two-mica granitoid rocks, however, the composition of the primary white mica is both titaniferous and, for those rocks that lack an aluminosilicate, ferriceladonitic (Best *et al.* 1974, Guidotti 1978, Anderson *et al.* 1980, Miller *et al.* 1981).

For these intrusive rocks, the mole % celadonite is highest in primary muscovites of the older garnet-biotite granodiorite, ranging from 24.2 to 32.5%, but is only slightly less in all other rocks (all peraluminous sills and the older two-mica adamellite), ranging from 19.5 to 29.8%. In all cases, the paragonite content is low (less than 3.0 mole %, usually less than 1.0%). Assuming dioctahedral stoichiometry, the celadonite end-member is high in Fe³⁺ and Ti and approaches the composition $K(Mg_{0.8}Ti_{0.2})Fe^{3+}(Si_{3.6}Al_{0.4})O_{10}(OH)_2$. In contrast, the composition of the celadonite end-member of Ti-depleted secondary muscovite approximates $KMgFe^{3+}Si_4O_{10}(OH)_2$. Although there is commonly a compositional gap, the range of composition of the celadonite end-member from primary to secondary muscovite in the two-mica granitoid rocks in this and other studies (Anderson *et al.* 1980, Miller *et al.* 1981, Best *et al.* 1974) can best be described by the general formula $K(Mg_{1-x}Ti_x)Fe^{3+}(Si_{4-2x}Al_{2x})O_{10}(OH)_2$, where *x* ranges from 0.2 to 0.

Use of muscovite as a petrogenetic indicator

Many previous workers have recognized that the presence of primary muscovite in granitic rocks allows the estimation of a lower limit of pressure (hence minimum depth) of crystallization. This aspect, true only for cases involving end-member muscovite, has been chemographically explored by Thompson & Algor (1977) and Thompson & Tracy (1979). Some workers incorrectly place this lower limit at the intersection of the water-saturated granite solidus and the reaction $Mu + Qz = Ksp + Sill + H_2O$ (e.g., Carmichael *et al.* 1974, p. 264). This reaction, which describes the upper stability of muscovite in the presence of quartz, does not intersect the H₂O-saturated solidus in P-T-X space. As shown in Figure 5A, the true lower limit is the intersection of the melting curve and the lower temperature reaction (L): $Mu_{ss} + Ab_{ss} + Qz = Ksp_{ss} + Als + V$. Hence, only silicate liquids in divariant fields III, IV and V can

coexist with end-member muscovite. This system (Fig. 5A) involves four components projected from SiO_2 and can have only one invariancy; six univariant reactions emanate from the derived bundle. A simplified view, projected from H_2O (for water-saturated liquids), is shown in Figure 5B.

As we are not dealing with a pure system for muscovite, feldspar or melt, the additional components of anorthite (Fig. 5C) and celadonite (Fig. 5D) have been added. In both cases, no new phases are created but rather a solid solution is formed. In the depicted systems of four components and five phases only a single uni-

variancy can exist, all other reactions being degenerate.

With anorthite added (Fig. 5C), the only non-degenerate reaction is $\text{Mu} + \text{L} = \text{Ksp} + \text{Pl} + \text{Als} + \text{V}$, which replaces the previous (Ab) equilibria. The composition of plagioclase in this univariacy changes continuously and approaches albite at the degenerate invariancy. All other curves are degenerate and represent the initiation of a family of higher-temperature curves describing continuous reactions involving more calcic plagioclase. It is important to note that magmatic muscovite (coexisting with liquid L) is still restricted to fields III, IV, and V.

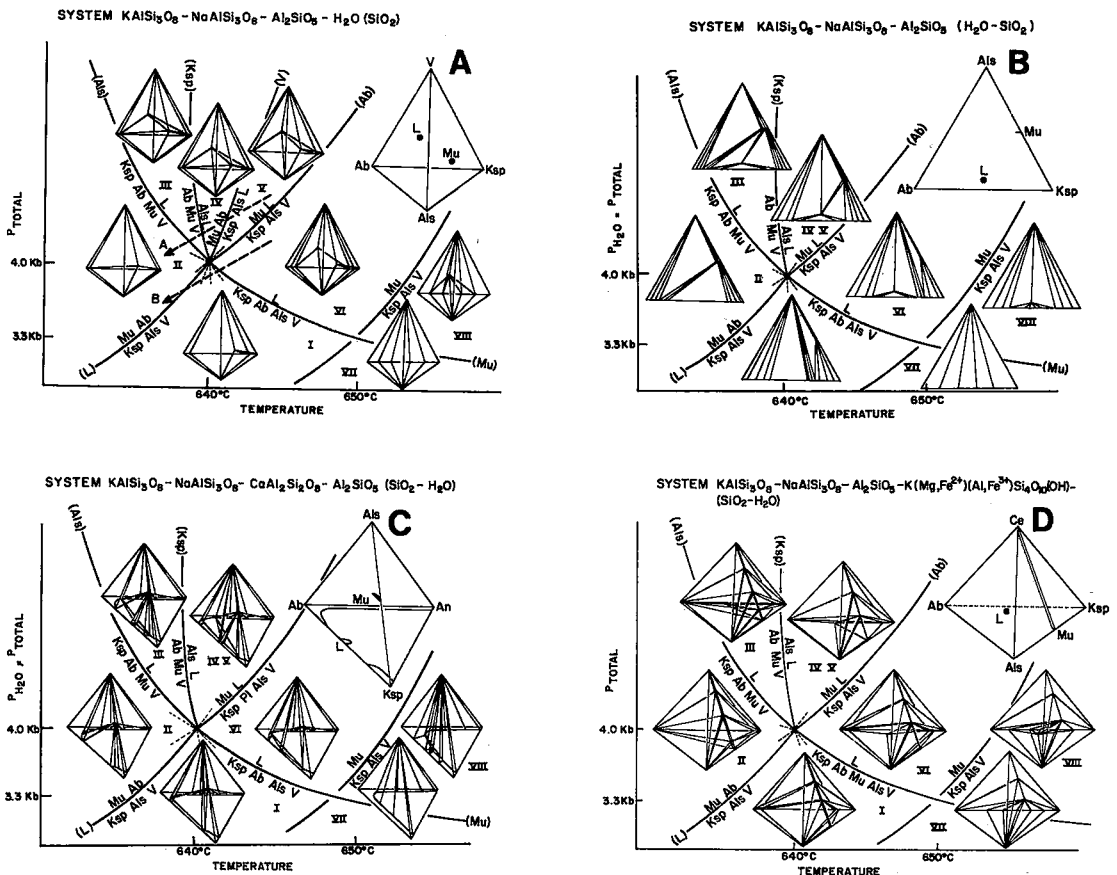


FIG. 5. Graphic analysis of the system $\text{SiO}_2\text{-KAlSi}_3\text{O}_8\text{-NaAlSi}_3\text{O}_8\text{-CaAl}_2\text{Si}_2\text{O}_8\text{-Al}_2\text{SiO}_5\text{-K(Mg,Fe}^{2+})\text{(Al,Fe}^{3+})\text{Si}_4\text{O}_{10}(\text{OH})_2\text{-H}_2\text{O}$ to describe phase relations in muscovite-bearing granitic melts. Phases include alkali feldspar Ksp, albite Ab, plagioclase Pl, muscovite Mu, an Al_2SiO_5 polymorph Als, granitic melt L and H_2O V. A. System $\text{KAlSi}_3\text{O}_8\text{-NaAlSi}_3\text{O}_8\text{-Al}_2\text{SiO}_5\text{-H}_2\text{O}$ projected from SiO_2 . End-member muscovite $\text{KAl}_2(\text{Si}_3\text{Al})\text{O}_{10}(\text{OH})_2$ coexists with granitic melt only for path A (fields III-V). B. Same system projected from H_2O . C. Addition of the component anorthite generates a single univariant reaction $\text{Mu} + \text{L} = \text{Ksp} + \text{Pl} + \text{Als} + \text{V}$. All other equilibria are degenerate. D. Addition of celadonite end-member $\text{K(Mg,Fe}^{2+})\text{(Al,Fe}^{3+})\text{Si}_4\text{O}_{10}(\text{OH})_2$ as a component generates a single univariant reaction $\text{Ksp} + \text{Ab} + \text{Mu} + \text{Als} + \text{V} = \text{L}$. All other equilibria are degenerate. Note that the equilibrium between the granitic melt and celadonitic muscovite has no lower pressure limit.

However, the effect of adding the celadonite component is dramatic (Fig. 5D): it allows the mica to coexist with liquids at much lower pressures. The only true univariacy in this system is the wet-melting curve $Ksp + Ab + Mu + Als + V = L$ (quartz-saturated), which replaces the previous (Mu) univariacy. All other curves are degenerate and again represent the initial curve of a family of higher temperature curves that describe continuous reactions involving sequentially more celadonitic muscovite. Of interest is the composition of muscovite in the only true univariant reaction ($Ksp + Ab + Mu + Als + V = L$): muscovite changes from being pure $KAl_2(Si_3Al)O_{10}(OH)_2$ at the degenerate invariacy to being increasingly celadonitic with lower pressure and higher temperature. The composition of celadonitic muscovite at any selected point on this solidus curve would be the same as the composition of muscovite in a contour of any of the displaced degenerate reactions [(L), (Als), (Ksp), (Ab)] that intersect the solidus at that point.

This implies that celadonite should extend the stability of muscovite in the granite system, which is consistent with our empirical studies showing that retrograded muscovite in granitic rocks is less celadonitic. This conclusion is at odds with Velde's (1965, 1967, 1972) interpretation of his experimental data but, as noted by Guidotti & Sassi (1976), Velde's careful study defined the solubility limit of celadonite in muscovite, not the stability limit of celadonitic muscovite. Velde calibrated the breakdown of celadonitic muscovite of known composition to less celadonitic muscovite of unknown composition + biotite + feldspar + quartz. The product assemblage corresponds to that of two-mica granites. Its stability field was not studied, but in view of this and other studies (e.g., Miller *et al.* 1981), it must extend to magmatic conditions.

On thermodynamic grounds, the reactions $Mu + Qz = Ksp + Als + V$ and $Mu_{ss} + Ab_{ss} + Qz = Ksp_{ss} + Als + V$ should shift to higher temperatures, as the activity of $KAlSi_3O_8$ in alkali feldspar is greater than the activity of $KAl_2Si_3AlO_{10}(OH)_2$ in the white mica of two-mica granites. The latter reaction would be further shifted to higher temperatures (lower pressures of intersection with the solidus) since the activity of $NaAlSi_3O_8$ in plagioclase also is less than one.

On geological grounds, more and more shallow-level muscovite-bearing plutons are being recognized. Some two-mica granites have been emplaced in terrains bearing cordierite (Miller

& Stoddard 1978) or andalusite + cordierite (Clarke *et al.* 1976, Clarke & Halliday 1980) as well as in structural horizons that could not have had more than 5 km of cover (Keith *et al.* 1980, S.B. Keith, pers. comm. 1980). Hence, it seems clear that muscovite-celadonite solutions may be stable phases in epizonal granitic liquids.

As the above analysis shows that the white mica on the H_2O -saturated solidus becomes more celadonitic with lower pressure, it should be possible to place constraints on this parameter based on the displacement of the experimental stability curves for the pure system as a function of compositions of the phases involved. The uncertainty in doing this is large, as (1) there is much variability in experimental results for $Mu + Qz$ stability (Thompson 1974) due largely to the polymorphic state of the Al_2SiO_5 phase and the extent of ordering in the feldspars (Chatterjee & Johannes 1974, Helgeson *et al.* 1978), (2) the important discontinuous reaction $Mu_{ss} + Ab_{ss} + Qz = Ksp_{ss} + Sill + H_2O$ has not been experimentally studied, and its position in P-T space is based on field calibrations (Thompson 1974) and (3) correct activity expressions for muscovite-celadonite solutions are unknown.

We have calculated the displacement in the muscovite stability curves utilizing the expression of Skippen (1977), which allows for an "equilibrium state of disorder" in the feldspar (Helgeson *et al.* 1978), modified for activities of the phases. For muscovite, we have used an ideal multisite mixing model similar to the plagioclase model 1 of Kerrick & Darken (1975) where

$$a_{Mu} = (X_K^{XII}) (X_{Al}^{VI})^2 \left[\left(\frac{Si}{Si + Al^{IV}/0.75} \right)^3 \left(\frac{Al^{IV}}{Si + Al^{IV}/0.25} \right) \right].$$

The activity of $KAlSi_3O_8$ in alkali feldspar was calculated using the Margules parameters of Thompson & Waldbaum (1969), and fugacity coefficients for H_2O were taken from Burnham *et al.* (1969).

The calculated curves intersect the solidus curve for adamellite-granodiorite H_2O -saturated melts at about 2.6–3.1 kbar, which corresponds to 9.6–11.5 km. We consider a water-saturated solidus appropriate, as the synkinematic adamellite-granodiorite sills are commonly pegmatitic in their interiors. These estimates are considered approximate owing to uncertainties mentioned above; actual depths may be even less in view of above geological observations that indicate a

shallow level of intrusion for other similar muscovite-bearing plutons.

Biotite

Mylonitization has generally not affected the primary composition of biotite in the two-mica intrusive bodies. Retrograded biotite in the matrix is systematically depleted in Ti and green in color and is thus easily distinguishable from the brown biotite in the matrix and porphyroclasts that have retained magmatic compositions. Hence, the latter can be utilized to estimate intensive parameters during intrusion and crystallization.

The primary biotites of all intrusive rocks are similar in composition. The biotites in the metaluminous rocks tend to be slightly richer in Mg and poorer in Al relative to those in the peraluminous rocks [$Fe/(Fe + Mg) = 0.414-0.502$ and $0.460-0.547$, respectively]. As this mica coexists with alkali feldspar and magnetite in all cases, its stability is a function of phase composition, temperature, fugacities of oxygen and water and total pressure (Wones & Eugster 1965). Assuming $P(H_2O) = P_{total}$, the stability of these biotites can be contoured in $T-f(O_2)$ space (Fig. 6) at specified pressures once expressions for activities of biotite, feldspar, and magnetite and $f(H_2O)$ are determined. For shallow intrusive bodies, the composition of biotite acts simply as an oxygen barometer. We have chosen a lower limit of pressure to be 2 kbar (see muscovite section) and an arbitrary upper limit of

4 kbar, and determined the fugacities of H_2O for each pressure as a function of temperature with the fugacity coefficients of Burnham *et al.* (1969). The activity of magnetite was assumed to be the mole fraction of Fe_3O_4 in the spinel phase; we calculated the activity of $KAlSi_3O_8$ in alkali feldspar using the Margules parameters of Thompson & Waldbaum (1969). We had to use a range of composition for both magnetite and alkali feldspar, as these two phases had thoroughly re-equilibrated with mylonitization. Biotite was treated as an ideal solution (Goodman 1976); the activity of annite in biotite was calculated as

$$a_{Ann} = (X_{Fe}/\Sigma OCT)^3 \left(\frac{K}{K + Na} \right) \left(\frac{F}{F + Cl + OH} \right)^2$$

The results are shown in Figure 6, where the contours for the most magnesian of the metaluminous biotites occur at a slightly higher fugacity of oxygen relative to the most iron-rich biotite of the peraluminous intrusive rocks. As the plot has both a temperature axis and pressure contours, the solidus field for water-saturated adamellitic to tonalitic liquids that would be in equilibrium with such biotites can also be plotted. Hence, this determines a window in $P-T-f(O_2)$ space for the intrusive rocks, provided they were water-saturated during final stages of crystallization. This should be a good approximation.

These calculations indicate that crystallization

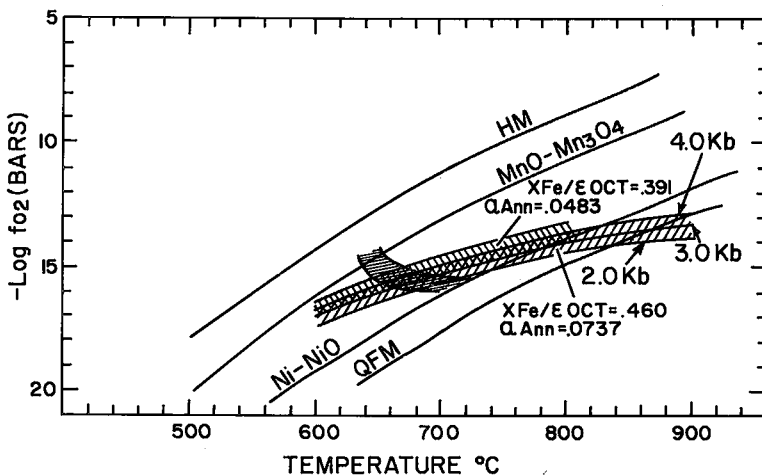


FIG. 6. Stability fields of biotite over a range of $P(H_2O)$ for metaluminous (upper set) and peraluminous (lower set) granitic rocks. Densely ruled region is a wet solidus field for adamellitic to tonalitic melts in equilibrium with these biotites; this region defines a window in $P-T-f(O_2)$ space for conditions of crystallization.

occurred under fairly oxidizing conditions. This is consistent with the Fe-Ti oxide mineralogy of these rocks, as ilmenite is rare to absent (Ishihara 1977). This factor sets these peraluminous granites apart from highly peraluminous granites (of S type), which seem to crystallize at lower fugacities of oxygen (*ca.* QFM buffer) and have a predominance of ilmenite over magnetite (Wones 1979, Hine *et al.* 1978).

Garnet

The composition of garnet in peraluminous sills and in older plutons is remarkably constant. Almandine is the most abundant component (42.6–47.4 mole %), with the remainder principally spessartine and grossular in subequal proportions (Fig. 7). The amount of pyrope (5.4–12.8%) and andradite (2.2–6.2%) end-members is consistently low. In general, the garnets are not zoned except in large crystals (3–6 mm) that have rims matching the composition of smaller garnets in the same rock. The zonation involves a core-to-rim depletion in Mn, which has been noted for garnet from other two-mica granitoid rocks (Miller & Stod-

dard 1978). For the Whipple Mtn. rocks, the solution scheme is $2\text{Mn} = \text{Ca} + \text{Fe}$ (older garnet-biotite granodiorite pluton) and $\text{Mn} = \text{Ca}$ (garnet-two-mica granodiorite sill).

Garnets in granitic rocks have been considered by some to be xenocrysts (see review by Venum & Meyer 1979). This is quite unlikely in this case, as the country-rock gneisses at the level of intrusion of these bodies are largely devoid of garnetiferous units. Garnets that are present occur in thin pelitic schist interlayers; these garnets are quite different in composition ($\text{Al}_{74.4-77.7} \text{Py}_{15.5-16.5} \text{Sp}_{1.7-3.9} \text{Gr}_{5.0-6.0}$).

Although intact crystals are broken and dismembered by mylonitization, careful probe traverses have revealed no overgrowths or sharp enrichments at the rims. Apart from a few fractures filled with chlorite, the garnets seem particularly resistant to change. Hence, we consider the garnets to be purely igneous in composition. Garnets in other two-mica granite intrusive rocks of the Cordilleran metamorphic complexes are likewise known to be spessartine-rich (Miller & Stoddard 1978, Ghent *et al.* 1979), although the garnets of this study also contain

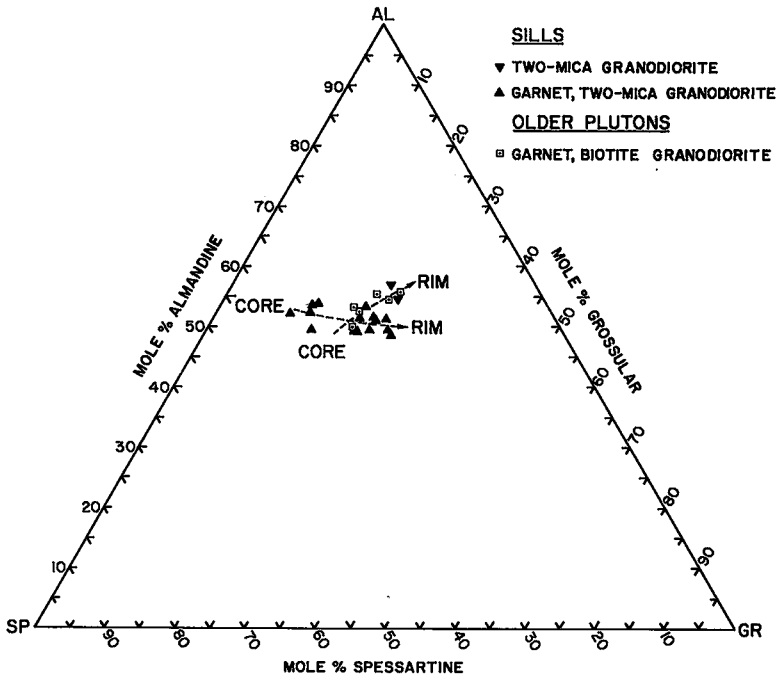


FIG. 7. Composition of primary garnets from older plutons (open symbols) and synkinematic sills (closed symbols) in terms of mole % almandine, grossular and spessartine components. Proportions of remaining components (pyrope and andradite) total less than 15 mole %. Note minor core-to-rim zonation.

significant amounts of the grossular component. Experiments by Green (1977) have shown that whereas almandine garnet indicates pressures greater than 7 kbar, garnets with 20–25 mole % spessartine are stable to pressures of less than 3 kbar. Green's work is certainly at a reconnaissance stage and subject to modification (Clemens & Wall 1981), but his conclusions are consistent with the low pressures we calculated in the above section on muscovite.

The temperature dependence of Mg–Fe partitioning between garnet and biotite is well known (Ferry & Spear 1978), but their model is inapplicable to our compositions, as it does not correct for additional components in either phase. Goldman & Albee (1977) have developed a more general thermometer based on correlation with temperatures from $^{18}\text{O}/^{16}\text{O}$ partitioning between quartz and magnetite; they make corrections for additional components in both biotite and garnet. Our calculated temperatures average $738 \pm 115^\circ\text{C}$. Considering present uncertainties in calibration, these results seem reasonable and further indicate that the garnets and biotites have retained magmatic compositions.

The core–rim depletion in Mn mentioned

above is interesting. Since garnet has such a strong affinity for Mn, we suggest that a depletion model may be appropriate, with initial crystallization of garnet causing early depletion of this component in the original melt.

ROCK CHEMISTRY

Compositional data for the older plutons and synkinematic sills are given in Tables 1 and 2 and Figures 8 and 9. For comparative purposes, data from the late kinematic plutons (Krass 1980) are also shown in Figure 8. One remarkable feature is the compositional similarity of all intrusive rocks, regardless of relative age and degree of alumina saturation. The lack of iron enrichment and a high alkali–lime index (Fig. 8) are features common to synorogenic magmatic suites. Yet, on closer inspection, the compositional trends (Fig. 9) differ markedly from other peraluminous and metaluminous calc–alkaline complexes; the characteristics of this suite must somehow be intrinsic to a common line of melt generation that transcends the sequential development of tectonic events.

The Whipple peraluminous suite is not strongly saturated with alumina, and does not fit the

TABLE 1. COMPOSITION OF METALUMINOUS GRANITOID ROCKS

Sample	Hornblende–Biotite Quartz Diorite		Porphyritic Granodiorite			Biotite Granodiorite		
	WV-17	MR-292	W78-53a	W78-49b	W78-49a	W-79-10	W-79-16	W-79-26
SiO ₂ ¹	60.82	62.64	66.65	67.08	68.78	69.43	71.62	71.58
TiO ₂	.66	.74	.51	.37	.42	.42	.25	.23
Al ₂ O ₃	16.87	17.08	16.86	16.87	15.97	15.86	15.60	15.66
FeO ²	5.25	4.09	2.74	2.29	2.50	2.15	1.42	1.28
MgO	2.77	2.36	1.16	.78	.72	.82	.50	.39
MnO	.117	.084	.038	.010	.012	.037	.056	.015
CaO	5.46	4.73	2.93	2.79	3.07	3.05	2.33	2.19
Na ₂ O	4.01	4.06	5.20	5.03	4.76	5.16	4.85	5.38
K ₂ O	2.11	1.74	2.86	3.25	2.73	2.59	3.37	2.77
L.O.I. ³	.93	.95	.61	.62	.45	.80	.38	.59
TOTAL	99.01	98.45	99.56	99.09	99.41	100.32	100.38	100.09
K ₂ O+Na ₂ O	6.12	5.80	8.06	7.82	7.49	7.75	8.22	8.15
FeO/FeO+MgO	.655	.634	.703	.746	.776	.724	.740	.766
"Al" ⁴	.897	.995	.993	1.001	.976	.942	.984	.989
K ₂ O/Na ₂ O	.526	.429	.550	.646	.574	.502	.695	.515
Ba	1065	1202	1114	1171	1344	1101	1458	1141
Rb	60.0	38.4	63.6	63.6	45.5	53.2	78.6	47.6
Sr	919	1461	796	822	823	884	785	716
Ba/Sr	1.16	.823	1.40	1.42	1.63	1.25	1.86	1.59
Ba/Rb	17.8	31.3	17.5	18.4	29.5	20.7	18.6	24.0
Rb/Sr	.0653	.0263	.0799	.0774	.0553	.0602	.1001	.0665
K/Rb	292	376	373	424	498	404	356	483
QZ	10.11	15.01	14.44	15.48	20.02	19.25	22.03	21.81
OR	12.68	10.52	16.92	19.34	16.26	15.29	19.84	16.33
AB	36.63	37.31	46.75	45.48	43.09	46.29	43.38	48.21
AN	22.19	23.80	14.25	13.94	14.27	12.47	10.81	10.39
CD	0.00	0.00	0.00	0.01	0.00	0.00	0.00	0.00
DI	4.30	0.18	0.25	0.00	0.87	2.12	0.56	0.36
HY	13.16	12.11	6.68	5.24	4.90	4.00	3.03	2.58
MT	0.00	0.00	0.00	0.00	0.00	0.00	0.00	0.00
IL	0.94	1.06	0.71	0.52	0.59	0.58	0.35	0.32
AN/(AB+AN)	0.3773	0.3895	0.2336	0.2346	0.2488	0.2122	0.1995	0.1773

¹ Analyses done at U.S.C. Petrochemistry Laboratory; Major elements as wt. %; Ba, Rb, Sr as ppm

² All Fe as FeO

³ L.O.I. = Loss on Ignition at 1000°C

⁴ "Al" = Molecular proportions of Al₂O₃/(CaO + Na₂O + K₂O)

THE CANADIAN MINERALOGIST

TABLE 2. COMPOSITION OF PERALUMINOUS AND RELATED INTRUSIVE ROCKS

A. Older plutons												
Sample	Garnet-Biotite Granodiorite										Two-Mica Adakinite	
	MR-165	MR-162	MR-139	W198	MR-195	MR-194	W79-132	W-79-74 ¹	W-79-74 ²	W-78-47	W78-46a	W78-46b
SiO ₂ ¹	61.09	61.80	62.08	64.68	66.93	67.90	68.75	68.89	69.80	71.93	72.66	73.37
TiO ₂	0.86	0.44	0.51	0.47	0.34	0.52	0.28	0.37	0.43	0.16	0.14	0.16
Al ₂ O ₃	18.42	18.53	17.61	17.73	16.78	16.80	15.28	14.47	14.81	14.78	15.07	14.37
FeO	3.94	3.54	3.82	2.38	2.37	2.56	2.83	1.75	1.68	1.34	1.70	0.82
MgO	1.69	1.56	1.58	1.24	0.96	1.09	0.87	0.62	0.80	0.46	0.53	0.34
MnO	0.09	0.06	0.10	0.04	0.01	0.03	0.15	0.03	0.30	0.24	0.04	0.09
CaO	5.79	5.83	5.80	4.98	4.10	2.45	2.71	1.79	1.80	2.66	2.49	1.93
Na ₂ O	4.42	4.79	4.41	4.48	4.06	4.32	3.72	2.76	2.88	3.83	3.80	3.90
K ₂ O	1.57	1.31	1.41	1.54	1.86	3.39	3.26	5.30	5.51	2.43	2.49	3.66
L.O.I. ³	0.97	1.07	1.01	0.99	0.69	0.60	0.76	0.83	0.80	1.07	1.02	0.74
TOTAL	98.52	98.87	98.30	98.45	98.54	98.76	98.33	98.74	98.37	98.52	99.94	99.21
K ₂ O/Na ₂ O	5.99	6.10	5.82	6.02	6.32	7.71	6.98	8.06	8.39	6.26	6.29	7.56
FeO/(FeO+MgO)	0.700	0.694	0.707	0.658	0.712	0.701	0.765	0.738	0.737	0.744	0.762	0.707
*Al ^{iv}	945	949	911	980	999	1038	1047	1070	1060	1082	1119	1035
K ₂ O/Na ₂ O	355	274	320	344	417	785	276	1.92	1.91	777	635	783
Ba	892	636	1348	927	1488	2464	1465	3592	3605	777	968	894
Rb	47.5	38.8	23.4	40.8	31.6	52.2	65.5	69.8	72.4	41	57.0	59.9
Sr	1096	1275	946	1037	908	580	679	905	930	715	674	392
Ba/Sr	0.814	0.499	1.45	0.894	1.64	4.25	2.16	3.97	3.88	1.09	1.44	2.00
Ba/Rb	18.8	16.39	27.27	22.7	47.1	47.2	22.4	51.5	49.8	15.8	17.0	8.78
Rb/Sr	0.0433	0.904	0.60	0.313	0.393	0.348	0.539	0.411	0.965	0.0687	0.0846	0.226
K/Rb	274	280	500	500	313	489	539	630	632	111	363	400
OZ	11.47	11.51	13.60	17.69	20.68	19.94	24.03	25.90	25.00	31.61	31.65	29.69
OR	7.46	7.87	8.53	9.28	11.21	20.39	19.89	32.95	33.65	14.92	14.92	22.04
AB	40.47	43.75	40.57	41.05	40.85	39.50	34.34	26.02	26.73	35.49	34.76	35.69
AN	26.31	25.64	24.70	24.22	20.69	12.38	13.83	9.32	9.21	13.32	12.59	9.76
CO	0.00	0.00	0.00	0.00	0.00	0.00	0.00	0.00	0.00	0.00	0.00	0.00
DI	2.39	2.22	3.83	0.80	0.05	0.00	0.00	0.00	0.96	1.27	1.78	0.84
HT	9.10	8.38	8.05	6.34	6.04	6.42	6.83	4.19	3.83	3.26	4.04	2.05
MT	0.00	0.00	0.00	0.00	0.00	0.00	0.00	0.00	0.00	0.00	0.00	0.00
IL	0.80	0.62	0.73	0.67	0.48	0.74	0.40	0.54	0.62	0.23	0.20	0.23
AN(AB+AN)	0.3940	0.3898	0.3784	0.3711	0.3363	0.2386	0.2870	0.2638	0.2562	0.2728	0.2658	0.2147

B. Major Syntectonic Intrusives														
Sample	Two-Mica Tonalite				Garnet-Two-Mica Granodiorite					Two-Mica Granodiorite				
	W18	W19	W129	MR24	MR47	W16	MR118	MR57	W79-241	W54	W79-183	W79-127B	W79-43B	W79127A
SiO ₂	65.27	67.99	68.51	69.72	69.82	70.17	70.51	71.36	72.45	72.49	66.37	70.20	71.50	71.51
TiO ₂	0.42	0.28	0.28	0.36	0.27	0.31	0.25	0.17	0.14	0.27	0.38	0.36	0.27	0.31
Al ₂ O ₃	17.08	16.87	16.59	16.11	15.55	16.39	15.19	15.30	14.98	15.30	16.93	16.12	15.82	15.28
FeO	3.22	2.91	2.10	1.57	1.56	1.51	1.08	0.86	0.84	0.84	2.07	1.66	1.41	1.47
MgO	1.44	1.05	0.88	0.66	0.68	0.66	0.42	0.37	0.32	0.32	1.25	0.67	0.67	0.59
MnO	0.020	0.049	0.056	0.017	0.113	0.094	0.125	0.099	0.134	0.092	0.074	0.040	0.016	0.036
CaO	4.40	3.70	3.48	2.08	2.76	2.94	2.65	2.05	2.17	1.99	4.99	2.67	2.48	2.21
Na ₂ O	4.33	4.30	4.15	5.41	4.06	4.72	3.95	4.81	4.09	3.85	4.22	3.05	2.98	4.84
K ₂ O	1.65	2.43	2.33	2.65	3.18	2.82	3.19	3.00	3.39	4.31	1.71	2.61	2.12	2.87
L.O.I. ³	1.16	0.59	0.72	0.80	0.80	0.80	0.80	0.80	0.80	0.80	0.70	0.49	0.58	0.47
TOTAL	99.05	99.77	98.00	99.08	99.24	99.58	99.12	98.50	99.53	99.43	99.09	100.18	99.96	99.12
K ₂ O/Na ₂ O	5.98	6.73	6.49	8.05	7.24	7.94	7.16	7.81	7.48	8.16	5.93	7.96	7.41	7.71
FeO/(FeO+MgO)	0.691	0.705	0.785	0.684	0.677	0.644	0.659	0.729	0.789	0.724	0.697	0.709	0.730	0.714
*Al ^{iv}	1010	1027	1001	1040	1030	1014	1029	1027	1045	1047	988	978	1020	1013
K ₂ O/Na ₂ O	381	565	562	490	783	598	808	624	829	1.12	405	488	401	593
Ba	41.7	44.1	37.9	38.4	92.3	1189	1651	1668	1087	884	1066	1410	1242	1430
Rb	932	833	735	648	648	582	660	801	577	498	45.1	57.9	25.2	69.4
Sr	1.15	2.08	1.87	3.46	1.44	2.04	2.50	2.08	1.88	1.78	1.05	1.40	1.37	1.83
Ba/Rb	25.8	39.3	36.3	75.8	13.0	25.6	23.5	33.2	21.3	10.1	23.6	24.4	22.5	20.5
Rb/Sr	0.0447	0.0529	0.0516	0.73	0.486	1.116	0.799	1.064	0.8828	0.886	0.0443	0.0573	0.0609	0.0889
K/Rb	318	443	510	573	345	503	377	485	551	407	315	374	319	343
OZ	18.66	20.76	24.23	20.42	23.84	22.03	25.51	24.50	27.52	26.34	20.26	19.74	23.74	23.98
OR	9.94	14.46	14.18	18.77	19.09	18.72	19.19	17.96	20.28	25.70	10.27	15.39	12.54	17.06
AB	39.66	38.89	38.40	40.60	40.94	42.56	43.78	37.12	34.89	36.52	38.52	47.81	47.55	43.73
AN	22.27	18.49	17.79	10.30	13.91	14.64	13.39	10.35	10.90	9.97	22.58	12.22	11.03	11.03
CO	0.00	0.00	0.00	0.00	0.00	0.00	0.00	0.00	0.00	0.00	0.00	0.00	0.00	0.00
DI	0.00	0.00	0.00	0.00	0.00	0.00	0.00	0.00	0.00	0.00	0.00	0.00	0.00	0.00
HT	8.67	6.52	4.98	3.37	5.23	3.58	4.90	0.00	0.00	0.00	0.45	0.78	0.00	0.00
MT	0.00	0.00	0.00	0.00	0.00	0.00	0.00	0.00	0.00	0.00	0.00	0.00	0.00	0.00
IL	0.80	0.39	0.40	0.51	0.38	0.24	0.44	0.35	0.24	0.20	0.54	0.50	0.38	0.43
AN(AB+AN)	0.3596	0.3223	0.3167	0.1738	0.2731	0.2561	0.2705	0.1914	0.2267	0.2222	0.3696	0.2035	0.2058	0.2015

C. Minor Intrusives													
Sample	Biotite Tonalite					Trondhjemitic Aplite							
	MR-244	MR-277	MR-057	MR-57b	W7853C	MR-275	W-79-51C	W-79-43a	MR273	W-79-63C	MR273	W-79-63C	
SiO ₂	68.99	69.14	69.19	69.24	69.62	72.05	72.92	73.20	73.62	74.27	72.05	74.27	
TiO ₂	0.38	0.29	0.43	0.41	0.35	0.02	0.05	0.05	0.06	0.07	0.05	0.07	
Al ₂ O ₃	16.49	16.34	15.68	16.08	15.57	15.57	15.60	15.73	15.98	15.79	15.98	15.79	
FeO	1.84	1.85	1.93	1.57	1.63	1.31	1.39	1.35	1.39	1.31	1.39	1.31	
MgO	0.81	0.75	0.76	0.77	0.73	0.076	0.015	0.015	0.010	0.010	0.010	0.010	
MnO	0.021	0.093	0.025	0.020	0.021	<0.001	0.018	0.018	0.001	0.039	0.001	0.039	
CaO	3.01	2.81	2.69	2.92	2.53	1.17	1.19	1.09	1.11	1.25	1.17	1.25	
Na ₂ O	4.22	4.95	4.45	5.19	4.78	3.17	3.19	2.09	2.11	2.44	3.17	2.44	
K ₂ O	2.44	2.65	3.12	2.12	2.03	1.13	1.04	1.43	1.46	1.76	1.13	1.76	
L.O.I. ³	0.59	0.58	0.50	0.50	0.50	0.35	0.38	0.28	0.30	0.28	0.30	0.28	
TOTAL	99.49	99.37	98.98	98.80	98.71	98.73	99.77	99.14	99.60	100.35	99.14	99.60	
K ₂ O/Na ₂ O	7.36	7.60	7.57	7.31	7.81	9.07	9.25	8.36	8.14	8.20	9.07	8.20	
FeO/(FeO+MgO)	0.694	0.712	0.717	0.671	0.691	0.904	0.959	0.961	0.955	0.932	0.961	0.955	

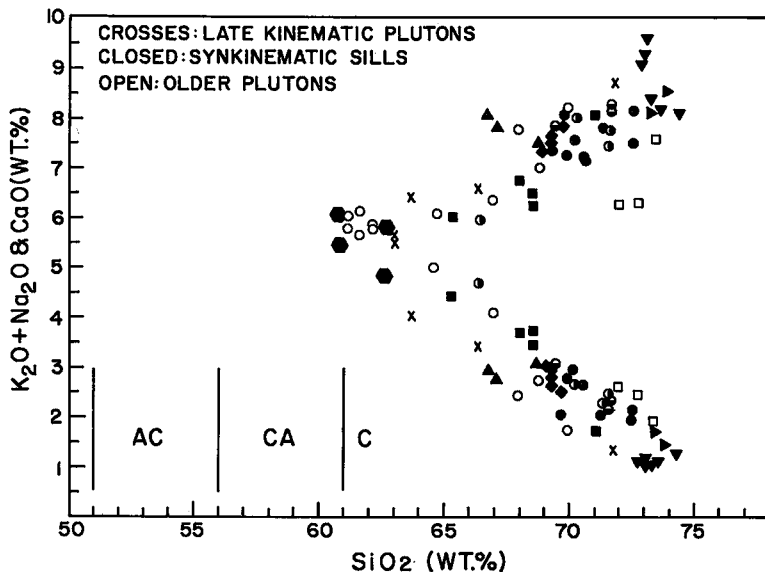


FIG. 8. Peacock plot of total alkalis and CaO versus SiO₂. Unit symbols as in Figure 3 with the addition of ▲ for trondhjemitic aplite sills, ◆ for biotite tonalite sills and x for late kinematic plutons.

definition of S-type granites (Chappell & White 1974). A parameter measuring the degree of alumina saturation is the molecular ratio $Al_2O_3 / (CaO + Na_2O + K_2O)$; whereas this value is commonly in the range of 1.09 to 1.46 for S-type granites, it is less than 1.13 for the Whipple rocks. The reason for high alumina-saturation, however, varies; Australian S-type granitoid rocks (Hine *et al.* 1978) owe their high degree of alumina saturation to low Na₂O, not high Al₂O₃. In contrast, Nova Scotia S-type granitoid rocks (de Albuquerque 1977) are highly peraluminous essentially because of high Al₂O₃. The Whipple rocks, like the Nova Scotia suite, are also very high in Al₂O₃, much higher so than the Australian suite. The weakly peraluminous nature is due to high values of Na₂O and CaO (Figs. 8, 9) and not to low Al₂O₃. Moreover, the metaluminous sills (porphyritic and biotite granodiorites, *i.e.*, *pgd* and *bgd* of Fig. 9) are not alumina-saturated as a result of even higher values of Na₂O.

Magma evolution

Presently we lack other trace-element (*e.g.*, REE) or isotopic data to quantify magmatic models totally, but our data coverage is adequate to identify potential lineages from separate parent melts and differentiation schemes. Although we feel that there are probably several magma-series involved, we emphasize that their

differences are not large. We suggest that at least six magma lineages correspond to the following major intrusive bodies: (1) the garnet-biotite granodiorite pluton, (2) the two-mica adamellite pluton, (3) the structurally deep hornblende-biotite quartz diorite sill, (4) the two-mica tonalite sill, (5) the two-mica granodiorite (two sills) and (6) the two upper biotite granodiorite sills. The amount of compositional variation within most of the intrusive bodies is minor and can be attributed to fractional crystallization of small amounts of plagioclase and lesser amounts of other constituent phases.

The only major change in magma composition occurs within the garnet-biotite granodiorite pluton. Over a silica range of 61.1 to 69.9% there is a depletion in Al, Fe, Mg, Ca, Na and Sr and an enrichment in K, Ba and Rb. As shown in Figure 9, this also involves a change from a metaluminous to peraluminous composition with increasing SiO₂. A significant increase in alumina saturation can occur by fractional crystallization of metaluminous phases such as hornblende, allanite and apatite. Hornblende occurs only in the most mafic members of this series, and allanite and apatite occur throughout. The decrease in Ca and Sr, the late decrease in Na and the increase in Ba suggest fractionation of plagioclase. Utilizing our microprobe data of the minerals involved, we can approximate

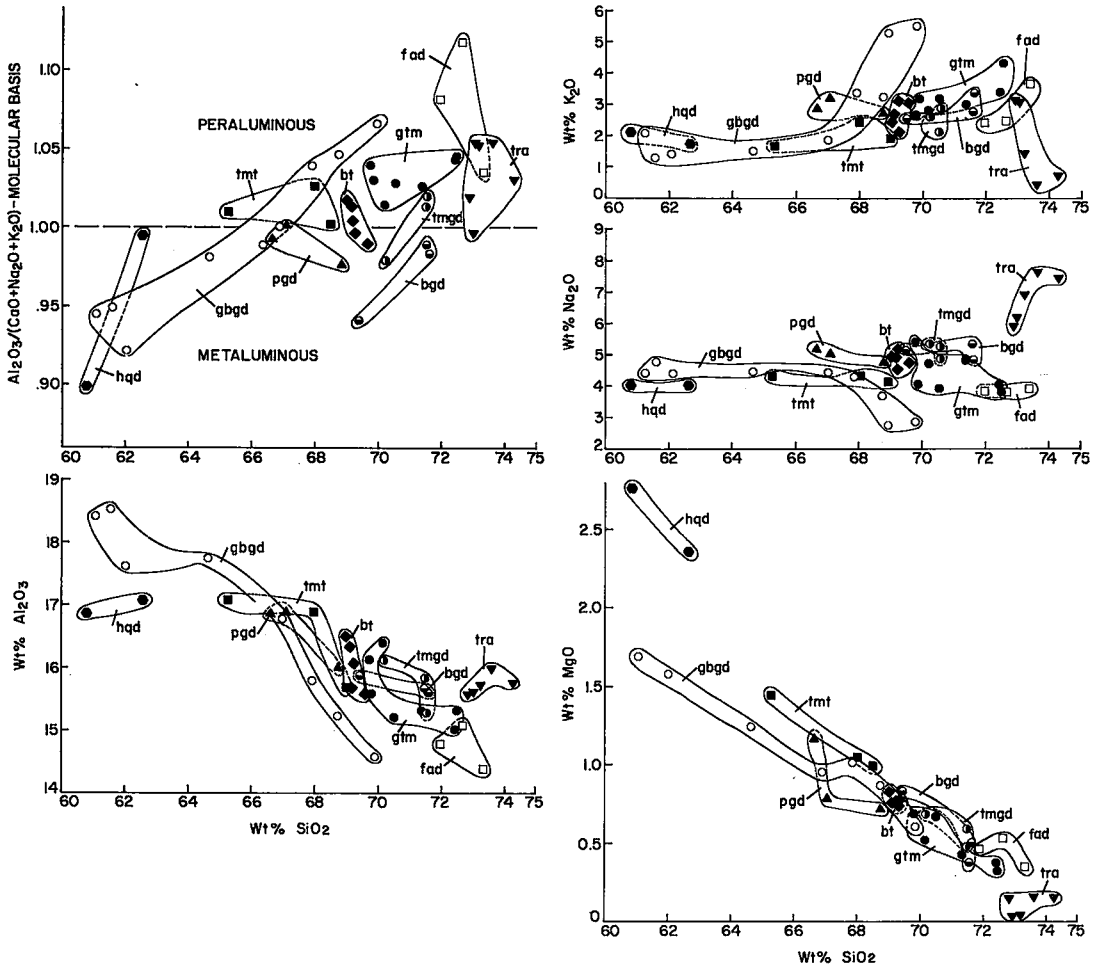


FIG. 9. Composition of older plutons and synkinematic sills; $\text{Al}_2\text{O}_3/(\text{CaO} + \text{Na}_2\text{O} + \text{K}_2\text{O})$ on a molar basis, Al_2O_3 , K_2O , Na_2O , and MgO versus SiO_2 . Symbols of units as in Figures 3 and 8.

about two-thirds of this series by 38% fractionation of plagioclase (An_{34} , 73.4%), hornblende (21.6%), biotite (2.3%), magnetite (1.4%), allanite or apatite (0.7%) and garnet (0.7%). This produces a model increase in the molar ratio of $\text{Al}_2\text{O}_3/(\text{CaO} + \text{Na}_2\text{O} + \text{K}_2\text{O})$ from 0.949 to 1.029, which is due to the removal of the hornblende + allanite + apatite fraction. We are unable to model adequately the last portions of this series with a fractional crystallization model, and suggest that late-stage volatile transfer may have played an active role. The REE abundance of members in this series should be a good test of the fractionation model, as a depletion in REE should result (Miller & Mittlefehldt 1979). Our microprobe analyses of allanite support this: there is a 17% decrease in concentration of La, Ce and Nd in allanite from

intermediate to most differentiated members of the series.

Collectively, the entire suite of older plutons, synkinematic sills and late kinematic plutons is so compositionally similar that differences in the nature of magma generation and source material must have been minor. Perhaps consistent with the calcic nature of the rocks, the Sr content (average 828 ppm) is high and unusual for peraluminous granites. Crustal sources with a significant metasedimentary component are often invoked for peraluminous melts (Hine *et al.* 1978, Clarke & Halliday 1980); although we consider this a possible source, the high Ca, Na and Sr of these melts then implies a large degree of melting. Our ongoing study is aimed at testing such preliminary models.

CONCLUSIONS

The rocks formed during these two intrusive episodes do not conform to the simple I-type versus S-type division of granitic rocks defined for other metamorphic belts (Chappell & White 1974). This suite is compositionally unique, and perhaps this reflects the intrinsic diversity that may eventually characterize peraluminous granitic complexes. The fact that this suite arose through magmatism coeval with two markedly different styles of deformation allows speculation that the two intrusive episodes are perhaps part of a near-continuum of igneous activity that spans a transition in the character of an evolving regime of crustal stresses. This conclusion depends upon whether the older plutonism is Mesozoic or Precambrian, and must await firmer age control. In view of the compositional features remarkably shared by the two intrusive groups, it seems clear that they have a common line of source material and nature of magma generation.

On mineralogical grounds, the celadonic nature of the primary muscovite is consistent with the absence of coexisting aluminosilicates and, in view of the chemographic analysis presented above, also is consistent with a depth estimate of 9.6–11.5 km (2.6–3.1 kbar). The Mn-rich composition of coexisting garnet may also be compatible with a shallow depth of intrusion. The low activity of annite noted in biotite and garnet–biotite geothermometry imply crystallization temperatures in the range 660–740°C under fairly oxidizing conditions (*ca.* Ni–NiO and MnO–Mn₂O₄ buffer curves). The latter aspect is also suggested by the Fe–Ti oxide mineralogy, specifically the near-absence of ilmenite.

At present we do not understand the origin of the Late Cretaceous mylonitization event. The spatial association of the sills with deformation is strong, and yet the sills cannot be the cause of the deformation, as major mylonitic gneiss sections occur devoid of sills both on strike with the intrusive bodies and structurally below the lowest sill, the hornblende–biotite quartz diorite. The mylonitized section involves a minimum structural thickness of 3.9 km, the bottom of which is not exposed. Both deformation and magma genesis are potentially separate manifestations of the same tectonic environment (Keith 1978), which may imply the generation and rise of melts derived in the crust, that intruded forcefully and spread laterally into a major zone of upper crustal strain.

ACKNOWLEDGEMENTS

This work has been funded by NSF grant EAR77–09695 to the senior author and G.A. Davis. We particularly acknowledge the help of G.A. Davis, who introduced the senior author to the Whipple Mountains and, as a field companion, critical reviewer and coworker, has worked closely with the authors on many aspects of this study. In addition, our mapping project in the central Whipple Mountains was made possible by Keith Howard and the U.S. Geological Survey, who flew in by helicopter our water and base camp supplies. Moreover, further helicopter support during the spring of 1980 allowed us to reach the deepest portions of this generally inaccessible range. Discussions with R.L. Armstrong, John T. Cheney, Eric G. Frost and Valerie Krass and critical reviews by D. Barrie Clarke, Simon K. Hanmer, Stan B. Keith and Calvin F. Miller proved invaluable. Miss Whitney A. Moore did many of our rock analyses and Paul Adams aided in the initial aspects of our microprobe study. Miss Terry E. Cameron point-counted most of our samples. Sharon Wallace did an admirable job of typing an exceedingly rough manuscript, and most of the figures were drafted by Janet Dodds.

REFERENCES

- ALBEE, A.L. & RAY, L. (1970): Correction factors for electron probe microanalysis of silicates, oxides, carbonates, phosphates, and sulfates. *Anal. Chem.* **42**, 1408–1414.
- ANDERSON, J.L. (1980): Mineral equilibria and crystallization conditions in the Late Precambrian Wolf River rapakivi massif, Wisconsin. *Amer. J. Sci.* **280**, 289–332.
- , CULLERS, R.L. & VAN SCHMUS, W.R. (1980): Anorogenic metaluminous and peraluminous granite plutonism in the mid-Proterozoic of Wisconsin, U.S.A. *Contr. Mineral. Petrology* **74**, 311–328.
- , DAVIS, G.A. & FROST, E.G. (1979a): Field guide to regional Miocene detachment faulting and Early Tertiary (?) mylonitization, Whipple–Buckskin–Rawhide Mountains, southeastern California and western Arizona. In *Geologic Excursions in the Southern California Area* (P.L. Abbott, ed.). *Geol. Soc. Amer. Guidebook*, 109–133.
- , PODRUSKI, J.A. & ROWLEY, M.C. (1979b): Petrologic studies in the “suprastructural” and “infrastructural” crystalline rocks of the Whipple Mountains of southeastern California. *Geol. Soc. Amer. Abstr. Programs* **11**, 66.

- BENCE, A.E. & ALBEE, A.L. (1968): Empirical correction factors for the electron microanalysis of silicates and oxides. *J. Geol.* **76**, 382-403.
- BERNAS, B. (1968): A new method for decomposition and comprehensive analysis of silicates by atomic absorption spectrometry. *Anal. Chem.* **40**, 1682-1686.
- BEST, M.G., ARMSTRONG, R.L., GRAUSTEIN, W.C., EMBREE, G.F. & AHLBORN, R.C. (1974): Mica granites of the Kern Mountains pluton, eastern White Pine Country, Nevada: remobilized basement of the Cordilleran miogeosyncline? *Geol. Soc. Amer. Bull.* **85**, 1277-1286.
- BURNHAM, C.W., HOLLOWAY, J.P. & DAVIS, N.F. (1969): Thermodynamic properties of water to 1000°C and 10,000 bars. *Geol. Soc. Amer. Spec. Pap.* **132**.
- CARMICHAEL, I.S.E., TURNER, F.J. & VERHOOGEN, J. (1974): *Igneous Petrology*. McGraw-Hill, New York.
- CHAPPELL, B.W. & WHITE, A.J.R. (1974): Two contrasting granite types. *Pac. Geol.* **8**, 173-174.
- CHATTERJEE, N.D. & JOHANNES, W. (1974): Thermal stability and standard thermodynamic properties of synthetic $2M_1$ -muscovite $KAl_2[AlSi_3O_{10}(OH)_2]$. *Contr. Mineral. Petrology* **48**, 89-114.
- CLARKE, D.B. & HALLIDAY, A.N. (1980): Strontium isotope geology of the South Mountain batholith, Nova Scotia. *Geochim. Cosmochim. Acta* **44**, 1045-1058.
- , MCKENZIE, C.B., MUECKE, G.K. & RICHARDSON, S.W. (1976): Magmatic andalusite from the South Mountain batholith, Nova Scotia. *Contr. Mineral. Petrology* **56**, 279-287.
- CLEMENS, J.D. & WALL, V.J. (1981): Origin and crystallization of some peraluminous (S-type) granitic magmas. *Can. Mineral.* **19**, 111-131.
- DAVIS, G.A., ANDERSON, J.L., FROST, E.G. & SHACKELFORD, T.J. (1980): Mylonitization and detachment faulting in the Whipple-Buckskin-Rawhide Mountains terrane, southeastern California and western Arizona. In *Metamorphic Core Complexes* (M. Crittenden, G.H. Davis & P.J. Coney, eds.). *Geol. Soc. Amer. Mem.* **153**, 79-129.
- DAVIS, G.H. & CONEY, P.J. (1979): Geologic development of the Cordilleran metamorphic core complexes. *Geology* **7**, 120-124.
- DE ALBUQUERQUE, C.A.R. (1977): Geochemistry of the tonalitic and granitic rocks of the Nova Scotia southern plutons. *Geochim. Cosmochim. Acta* **41**, 1-13.
- DEWITT, E. (1980): Comment on "Geologic development of the Cordilleran metamorphic core complexes". *Geology* **8**, 6-7.
- ERNST, W.G. (1963): Significance of phengitic micas from low grade schists. *Amer. Mineral.* **48**, 1357-1373.
- FERRY, J.M. & SPEAR, F.S. (1978): Experimental calibration of the partitioning of Fe and Mg between biotite and garnet. *Contr. Mineral. Petrology* **66**, 113-117.
- GHEHT, E.D., KISTLER, R.W. & O'NEIL, J.R. (1979): Petrogenesis of Mesozoic garnet-two-mica granites of the Ruby Mountains, Nevada. *Geol. Soc. Amer. Abstr. Programs* **11**, 432.
- GOLDMAN, D.S. & ALBEE, A.L. (1977): Correlation of Mg/Fe partitioning between garnet and biotite with $^{18}O/^{16}O$ partitioning between quartz and magnetite. *Amer. J. Sci.* **277**, 750-767.
- GOODMAN, B.A. (1976): On the interpretation of the Mössbauer spectra of biotites. *Amer. Mineral.* **61**, 169.
- GREEN, T.H. (1977): Garnet in silicic liquids and its possible use as a P-T indicator. *Contr. Mineral. Petrology* **65**, 59-67.
- GUIDOTTI, C.V. (1978): Muscovite and K-feldspar from two-mica adamellite in northwestern Maine: composition and petrogenetic implications. *Amer. Mineral.* **63**, 750-753.
- , CHENEY, J.T. & GUGGENHEIM, S. (1976): Distribution of titanium between coexisting muscovite and biotite in pelitic schists from northwestern Maine. *Amer. Mineral.* **62**, 438-448.
- & SASSI, F.P. (1976): Muscovite as a petrogenetic indicator in pelitic schist. *Neues Jahrb. Mineral. Abh.* **127**, 97-142.
- HAXEL, G., WRIGHT, J.E., MAY, D.J. & TOSDAL, R.M. (1980): Reconnaissance geology of the Mesozoic and Lower Cenozoic rocks of the southern Papago Indian Reservation, Arizona: a preliminary report. *Ariz. Geol. Soc. Digest* **12**, 17-29.
- HELGESON, H.C., DELANY, J.M., NESBITT, H.W. & BIRD, D.K. (1978): Summary and critique of the thermodynamic properties of rock-forming minerals. *Amer. J. Sci.* **278-A**, 1-229.
- HINE, R., WILLIAMS, I.S., CHAPPELL, B.W. & WHITE, A.J.R. (1978): Contrasts between I- and S-type granitoids of the Kosciusko batholith. *Geol. Soc. Aust. J.* **25**, 219-234.
- ISHIHARA, S. (1977): The magnetite-series and ilmenite-series granitic rocks. *Mining Geol. (Kozan Chishitsu)* **27**, 293-305.
- KEITH, S.B. (1978): Paleosubduction geometries inferred from Cretaceous and Tertiary magmatic patterns in southwestern North America. *Geology* **6**, 516-521.

- , REYNOLDS, S.J., DAMON, P.E., SHAFIQUZZAH, M., LIVINGSTON, D.E. & PUSHKAR, P.D. (1980): Evidence for multiple intrusion and deformation within the Santa Catalina-Rincon-Tortolita metamorphic core complex. In *Metamorphic Core Complexes* (M. Crittenden, G.H. Davis & P.J. Coney, eds.). *Geol. Soc. Amer. Mem.* **153**, 217-267.
- KERRICK, D.M. & DARKEN, L.S. (1975): Statistical thermodynamic models for ideal oxide and silicate solid solutions, with application to plagioclase. *Geochim. Cosmochim. Acta* **39**, 1431-1442.
- KRASS, V.A. (1980): *Petrology of Upper Plate and Lower Plate Crystalline Terrane, Bowman's Wash Area of the Whipple Mountains, Southeastern California*. M.S. thesis, Univ. Southern California, Los Angeles.
- MARTIN, D.L., BARRY, W.L., KRUMMENACHER, D. & FROST, E.G. (1980): K-Ar dating of mylonitization and detachment faulting in the Whipple Mountains, San Bernardino County, California and the Buckskin Mountains, Yuma County, Arizona. *Geol. Soc. Amer. Abstr. Programs* **12**, 118.
- MILLER, C.F. & MITTFELDLT, D.W. (1979): Rare earth element depletion accompanying differentiation of felsic plutonic rocks. *Geol. Soc. Amer. Abstr. Programs* **11**, 479-480.
- & STODDARD, E.F. (1978): Origin of garnet in granitic rocks: an example of the role of Mn from the Old Woman-Piute Range, California. *Geol. Soc. Amer. Abstr. Programs* **10**, 456.
- , BRADFISH, L.J., DOLLASE, W.A. (1981): Composition of plutonic muscovite: genetic implications. *Can. Mineral.* **19**, 25-34.
- PODRUSKI, J.A. (1979): *Petrology of the Upper Plate Crystalline Complex in the Eastern Whipple Mountains, San Bernardino County, California*. M.S. thesis, Univ. Southern California, Los Angeles.
- ROBERT, J.-L. (1976): Titanium solubility in synthetic phlogopite solid solutions. *Chem. Geol.* **17**, 213-227.
- SKIPPEN, G.B. (1977): Dehydration and decarbonation equilibria. In *Application of Thermodynamics to Petrology and Ore Deposits* (H.J. Greenwood, ed.). *Mineral. Assoc. Can. Short Course Handbook* **2**, 66-83.
- STRECKEISEN, A. (1976): To each plutonic rock its proper name. *Earth Sci. Rev.* **12**, 1-33.
- THOMPSON, A.B. (1974): Calculation of muscovite-paragonite-alkali feldspar phase relations. *Contr. Mineral. Petrology* **44**, 173-194.
- & ALGOR, J.R. (1977): Model systems for anatexis of pelitic rocks. I. Theory of melting reactions in the system $\text{KAlO}_2\text{-NaAlO}_2\text{-Al}_2\text{O}_3\text{-SiO}_2\text{-H}_2\text{O}$. *Contr. Mineral. Petrology* **63**, 247-269.
- & TRACY, R.J. (1979): Model systems for anatexis of pelitic rocks. II. Facies series melting and reactions in the system $\text{CaO-KAlO}_2\text{-NaAlO}_2\text{-Al}_2\text{O}_3\text{-SiO}_2\text{-H}_2\text{O}$. *Contr. Mineral. Petrology* **70**, 429-438.
- THOMPSON, J.B., JR. & WALDBAUM, D.R. (1969): Mixing properties of sanidine crystalline solutions. III. Calculations based on two-phase data. *Amer. Mineral.* **54**, 811-838.
- THURN, L.C. (1980): *Structural Geology of the Southern Whipple Mountains, San Bernardino County, California*. M.S. thesis, Univ. Southern California, Los Angeles.
- VELDE, B. (1965): Phengitic micas: synthesis, stability, and natural occurrence. *Amer. J. Sci.* **263**, 886-913.
- (1967): Si⁴⁺ content of natural phengites. *Contr. Mineral. Petrology* **14**, 250-258.
- (1972): Celadonite mica: solid solution and stability. *Contr. Mineral. Petrology* **37**, 235-247.
- VENNUM, W.R. & MEYER, C.E. (1979): Plutonic garnets from the Werner batholith, Lassiter coast, Antarctic Peninsula. *Amer. Mineral.* **64**, 268-273.
- WONES, D.R. (1979): Intensive parameters during crystallization of granitic plutons. *Geol. Soc. Amer. Abstr. Programs* **11**, 543.
- & EUGSTER, H.P. (1965): Stability of biotite: experiment, theory, and application. *Amer. Mineral.* **50**, 1228-1278.

Received May 1980, revised manuscript accepted November 1980.